1521-009X/50/3/235–242$35.00
DRUG METABOLISM AND DISPOSITION

dx.doi.org/10.1124/dmd.121.000665
Drug Metab Dispos 50:235–242, March 2022

CYP2C8-Mediated Formation of a Human Disproportionate Metabolite of the Selective $Na_V1.7$ Inhibitor DS-1971a, a Mixed Cytochrome P450 and Aldehyde Oxidase Substrate[S]

Daigo Asano, Syoya Hamaue, Hamim Zahir, Hideyuki Shiozawa, Yumi Nishiya, Takako Kimura, Miho Kazui, Naotoshi Yamamura, Marie Ikeguchi, Takahiro Shibayama, Shin-ichi Inoue, Tsuyoshi Shinozuka, Toshiyuki Watanabe, Chizuko Yahara, Nobuaki Watanabe, and Kouichi Yoshinari

Drug Metabolism and Pharmacokinetics Research Laboratories (D.A., H.S., Y.N., M.K., N.Y., Ta.S., S.I., C.Y., N.W.), Translational Science Department (M.I.), R&D Planning and Management Department (Ts.S.), and Medicinal Safety Research Laboratories (T.W.), Daiichi Sankyo Co., Ltd., Tokyo, Japan; Organic and Biomolecular Chemistry Department, Daiichi Sankyo RD Novare Co., Ltd., Tokyo, Japan (S.H., T.K.); Quantitative Clinical Pharmacology and Translational Sciences, Daiichi Sankyo, Inc., Basking Ridge, New Jersey (H.Z.); and Laboratory of Molecular Toxicology, School of Pharmaceutical Sciences, University of Shizuoka, Shizuoka, Japan (K.Y.)

Received September 3, 2021; accepted December 6, 2021

ABSTRACT

Predicting human disproportionate metabolites is difficult, especially when drugs undergo species-specific metabolism mediated by cytochrome P450s (P450s) and/or non-P450 enzymes. This study assessed human metabolites of DS-1971a, a potent $Na_v1.7$-selective blocker, by performing human mass balance studies and characterizing DS-1971a metabolites, in accordance with the Metabolites in Safety Testing guidance. In addition, we investigated the mechanism by which the major human disproportionate metabolite (M1) was formed. After oral administration of radiolabeled DS-1971a, the major metabolites in human plasma were P450-mediated monoxidized metabolites M1 and M2 with area under the curve ratios of 27% and 10% of total drug-related exposure, respectively; the minor metabolites were dioxidized metabolites produced by aldehyde oxidase and P450s. By comparing exposure levels of M1 and M2 between humans and safety assessment animals, M1 but not M2 was found to be a human disproportionate metabolite, requiring further characterization under the Metabolites in Safety Testing guidance. Incubation studies with human liver microsomes indicated that CYP2C8 was responsible for the formation of M1. Docking simulation indicated that, in the formation of M1 and M2, there would be hydrogen bonding and/or electrostatic interactions between the pyrimidine and sulfonamide moieties of DS-1971a and amino acid residues Ser100, Ile102, Ile106, Thr107, and Asn217 in CYP2C8, and that the cyclohexane ring of DS-1971a would be located near the heme iron of CYP2C8. These results clearly indicate that M1 is the predominant metabolite in humans and a human disproportionate metabolite due to species-specific differences in metabolism.

SIGNIFICANCE STATEMENT

This report is the first to show a human disproportionate metabolite generated by CYP2C8-mediated primary metabolism. We clearly demonstrate that DS-1971a, a mixed aldehyde oxidase and cytochrome P450 substrate, was predominantly metabolized by CYP2C8 to form M1, a human disproportionate metabolite. Species differences in the formation of M1 highlight the regio- and stereoselective metabolism by CYP2C8, and the proposed interaction between DS-1971a and CYP2C8 provides new knowledge of CYP2C8-mediated metabolism of cyclohexane-containing substrates.

Introduction

The US Food and Drug Administration (FDA) guidance for industry on safety testing of drug metabolites defines disproportionate drug metabolites as "metabolites identified only in human plasma or metabolites present at higher levels in humans than in any of the animal test species" (FDA, 2020). If the area under the plasma concentration–time curve (AUC) of disproportionate metabolites accounts for more than 10% of total drug-related exposure and the exposure levels to disproportionate metabolites in humans are not covered by levels in test species, additional safety assessment is required. Several recent studies have reported disproportionate metabolites (Sharma et al., 2014; Schadt et al., 2018; Zheng et al., 2018; Surapaneni et al., 2021).

In general, in vivo human metabolites are predicted based on the results of in vitro incubation studies using human-derived materials, but in some cases over- or under-prediction of metabolites can be problematic, and predicting secondary metabolites and/or those resulting from non-cytochrome P450 (P450) enzyme-mediated metabolism is difficult (Anderson et al.,

This research was carried out with no funding.

No author has an actual or perceived conflict of interest with the contents of this article.

dx.doi.org/10.1124/dmd.121.000665.

[S] This article has supplemental material available at dmd.aspetjournals.org.

ABBREVIATIONS: AO, aldehyde oxidase; AUC, area under the plasma concentration–time curve; *CL*, clearance rate; HLM, human liver microsomes; ICH, International Conference on Harmonisation; LC-MS/MS, liquid chromatography–tandem mass spectrometry; MIST, Metabolites in Safety Testing; NADPH, nicotinamide adenine dinucleotide phosphate; Na_v, voltage-gated sodium channel; P450, cytochrome P450; PK, pharmacokinetic; QSAR, quantitative structure–activity relationship.

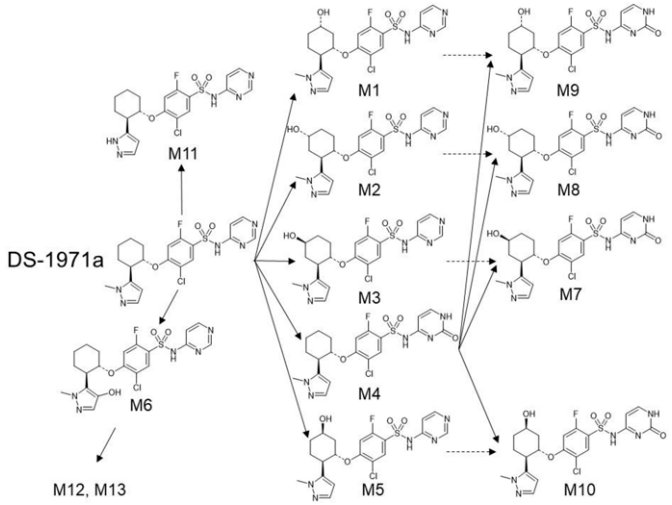

Fig. 1. Proposed metabolic pathways of DS-1971a from non-clinical studies. Quoted and modified from Asano et al. (2021). Solid and dashed arrows indicate the metabolic pathways with high and low possibility, respectively.

2009; Dalvie et al., 2009; Gross et al., 2009). Quantitative metabolite exposure in humans can be predicted using static and/or dynamic models (Nguyen et al., 2016; Obach et al., 2018; Callegari et al., 2020). Both methods can be used to predict metabolite exposure for P450 substrates in humans, but quantitative prediction of metabolite exposure for non-P450 enzyme substrates or mixed non-P450 enzyme and P450 substrates has had limited success (Lutz et al., 2010).

DS-1971a (Fig. 1) is a selective inhibitor of the $Na_v1.7$ voltage-gated sodium channel that is under development for the treatment of neuropathic pain (Shinozuka et al., 2020). The oral bioavailability of DS-1971a was moderate to high in monkeys (35%) and dogs (77%), and potent pain relief was observed in a neuropathic pain mouse model after oral administration. Mice and monkeys were selected as general toxicity animals from a viewpoint of pharmacological activity and AO metabolism. Non-clinical safety studies revealed a wide safety margin, with a no observed adverse effect level of 1000 mg/kg, the highest dose tested in 6- or 9-month repeated-dose toxicity studies in mice and monkeys (Shinozuka et al., 2020). In a Phase 1 single ascending dose study in healthy human subjects, DS-1971a was tolerable up to a dose of 1500 mg (https://clinicaltrials.gov/ct2/show/record/NCT02107885), and its effective human dose was estimated to be 400 mg based on exposure levels in a Phase 1 multiple ascending dose study (https://clinicaltrials.gov/ct2/show/NCT02190058). Thus, DS-1971a is a promising agent for pain relief with adequate safety.

Recently, we reported that DS-1971a is a mixed aldehyde oxidase (AO) and P450 substrate and that there is a marked species difference in DS-1971a metabolism between male mice and monkeys (Asano et al., 2021). After oral administration of DS-1971a, the most abundant metabolite in male mouse plasma was the AO metabolite M4, a monoxide at the pyrimidine ring, whereas that in male monkey plasma was the P450 metabolite M2, a monoxide at the cyclohexane ring (Fig. 1). The predominant metabolites after in vitro incubation of DS-1971a with human liver microsomes (HLM) and the human liver S9 fraction in the presence of nicotinamide adenine dinucleotide phosphate (NADPH) were the P450 metabolite M1, a monoxide at the cyclohexane ring, and its regioisomer M2. Considering that in vitro intrinsic clearance rates of DS-1971a in the human liver S9 fraction in the presence of NADPH were slightly or markedly decreased by the addition of hydralazine (an AO inhibitor) or 1-aminobenzotriazole (ABT; a pan-P450 inhibitor), respectively, the major metabolizing enzymes in humans, in vitro, are P450s and not AO (Asano et al., 2021). In addition, based on in vitro incubation studies, the in vivo major metabolite in humans was predicted to be M1 because the major circulating DS-1971a metabolites in mice (M4) and monkeys (M2) are consistent with the predominant metabolites produced in the same in vitro system. Thus, M1 was considered to be a potential human disproportionate metabolite, although there is some uncertainty about this prediction because AO is an unstable metabolic enzyme (Duley et al., 1985), and in vitro studies generally underestimate human clearance of AO substrates (Zientek et al., 2010).

In this study, we analyzed DS-1971a metabolites in human plasma, urine, and feces, collected as part of a human mass balance study, and found M1 and M2 to be the major DS-1971a metabolites in humans. Therefore, plasma M1 and M2 exposure levels were compared between humans and safety assessment animals to determine whether these metabolites were human disproportionate metabolites. Finally, we investigated the mechanism of M1 formation.

Materials and Methods

Chemicals and Reagents

The following were synthesized at Daiichi Sankyo Co., Ltd. (Tokyo, Japan): [^{14}C]DS-1971a (5-chloro-2-fluoro-4-{[(1*S*,2*R*)-2-(1-methyl-1*H*-pyrazol-5-yl)cyclohexyl]oxy}-*N*-(pyrimidin-4-yl)[U-$^{14}C_6$]benzenesulfonamide); DS-1971a (5-chloro-2-fluoro-4-{[(1*S*,2*R*)-2-(1-methyl-1*H*-pyrazol-5-yl)cyclohexyl]oxy}-*N*-(pyrimidin-4-yl)benzenesulfonamide); a stable-isotope-labeled racemic mixture of DS-1971a (5-chloro-2-fluoro-4-{[(1*RS*,2*SR*)-2-[1-(^{13}C,$^{2}H_3$)methyl-1*H*-pyrazol-5-yl]cyclohexyl]oxy}-*N*-(pyrimidin-4-yl)benzenesulfonamide); M1 (5-chloro-2-fluoro-4-{[(1*S*,2*R*,5*S*)-5-hydroxy-2-(1-methyl-1*H*-pyrazol-5-yl)cyclohexyl]oxy}-*N*-(pyrimidin-4-yl)benzenesulfonamide); M2 (5-chloro-2-fluoro-4-{[(1*S*,2*R*,4*R*)-4-hydroxy-2-(1-methyl-1*H*-pyrazol-5-yl)cyclohexyl]oxy}-*N*-(pyrimidin-4-yl)benzenesulfonamide); M3 (5-chloro-2-fluoro-4-{[(1*S*,2*R*,4*S*)-4-hydroxy-2-(1-methyl-1*H*-pyrazol-5-yl)cyclohexyl]oxy}-*N*-(pyrimidin-4-yl)benzenesulfonamide); M4 (5-chloro-2-fluoro-4-{[(1*S*,2*R*)-2-(1-methyl-1*H*-pyrazol-5-yl)cyclohexyl]oxy}-*N*-(2-oxo-1,2-dihydropyrimidin-4-yl)benzenesulfonamide); a racemic mixture of M5 (5-chloro-2-fluoro-4-{[(1*RS*,2*SR*,5*SR*)-5-hydroxy-2-(1-methyl-1*H*-pyrazol-5-yl)cyclohexyl]oxy}-*N*-(pyrimidin-4-yl)benzenesulfonamide); M6 (5-chloro-2-fluoro-4-{[(1*S*,2*R*)-2-(4-hydroxy-1-methyl-1*H*-pyrazol-5-yl)cyclohexyl]oxy}-*N*-(pyrimidin-4-yl)benzenesulfonamide); a racemic mixture of M7 (5-chloro-2-fluoro-4-{[(1*RS*,2*SR*,4*RS*)-4-hydroxy-2-(1-methyl-1*H*-pyrazol-5-yl)cyclohexyl]oxy}-*N*-(2-oxo-1,2-dihydropyrimidin-4-yl)benzenesulfonamide); a racemic mixture of M8 (5-chloro-2-fluoro-4-{[(1*RS*,2*SR*,4*SR*)-4-hydroxy-2-(1-methyl-1*H*-pyrazol-5-yl)cyclohexyl]oxy}-*N*-(2-oxo-1,2-dihydropyrimidin-4-yl)benzenesulfonamide); a racemic mixture of M9 (5-chloro-2-fluoro-4-{[(1*RS*,2*SR*,5*RS*)-5-hydroxy-2-(1-methyl-1*H*-pyrazol-5-yl)cyclohexyl]oxy}-*N*-(2-oxo-1,2-dihydropyrimidin-4-yl)benzenesulfonamide); a racemic mixture of M10 (5-chloro-2-fluoro-4-{[(1*RS*,2*SR*,5*SR*)-5-hydroxy-2-(1-methyl-1*H*-pyrazol-5-yl)cyclohexyl]oxy}-*N*-(2-oxo-1,2-dihydropyrimidin-4-yl)benzenesulfonamide); M11 (5-chloro-2-fluoro-4-{[(1*S*,2*R*)-2-(1*H*-pyrazol-5-yl)cyclohexyl]oxy}-*N*-(pyrimidin-4-yl)benzenesulfonamide); M12 (5-chloro-2-fluoro-4-({(1*S*,2*S*)-2-[(4*R*)-4-hydroxy-1-methyl-5-oxo-4,5-dihydro-1*H*-pyrazol-4-yl]cyclohexyl}oxy)-*N*-(pyrimidin-4-yl)benzenesulfonamide); and M13 (5-chloro-2-fluoro-4-({(1*S*,2*S*)-2-[(4*S*)-4-hydroxy-1-methyl-5-oxo-4,5-dihydro-1*H*-pyrazol-4-yl]cyclohexyl}oxy)-*N*-(pyrimidin-4-yl)benzenesulfonamide).

Pooled HLM, liver microsomes from mice, rats, dogs, and monkeys, and human liver S9 fraction were purchased from XenoTech (Kansas City, KS). Potassium phosphate buffer (KPB; pH 7.4), cDNA-expressing human P450 microsomes (control and CYP2C8), and NADPH-regenerating system solutions A and B were purchased from Corning (Woburn, MA). CYP1A2-, CYP2C8-, CYP2C9-, CYP2C19-, CYP2D6-, CYP3A4-SILENSOMES, and human plasma were purchased from Biopredic International (Saint Grégoire, France). Paclitaxel was purchased from Sigma-Aldrich (St. Louis, MO). Dimethylacetamide (DMA) was obtained from Nacalai Tesque (Kyoto, Japan). Saline was obtained from Otsuka Pharmaceutical Factory, Inc. (Tokushima, Japan). Methylcellulose 400 (MC) was obtained from FUJIFILM Wako Pure Chemical Corporation (Osaka, Japan).

Human Mass Balance Study

This study was approved by the Institutional Review Board and was performed in accordance with the ethical principles that have their origin in the Declaration of Helsinki, Good Clinical Practice, FDA regulations, and applicable local regulations. All subjects provided written informed consent.

An open-label study was conducted in six healthy male subjects, aged 18–55 years, by Worldwide Clinical Trials (San Antonio, TX). After post-meal administration of 400 mg/150 μCi [^{14}C]DS-1971a suspension, plasma, urine, and fecal samples were collected from subjects up to 192 hours after dosing. Sample radioactivity was measured using a liquid scintillation counter, and plasma and urinary concentrations of DS-1971a, M1, M2, M3, and/or M8 and M9 were quantified by liquid chromatography–tandem mass spectrometry (LC-MS/MS). Pharmacokinetic (PK) parameters were calculated using non-compartmental methods in WinNonlin 6.3 (Pharsight Corporation, Cary, NC). The excretion of total radioactivity into the urine and feces (% of dose) and the urinary excretion of DS-1971a, M1, and M2 (% of dose) were calculated by dividing the excreted radioactivity or the amount of DS-1971a, M1, and M2 by the radioactivity (150 μCi) or dose (400 mg) administered, respectively.

Metabolite Profiling in Human Plasma, Urine, and Feces

Plasma, urine, and fecal samples collected in the human mass balance study were used for metabolite profiling. Typically, after samples had been mixed with a twofold volume of acetonitrile, the mixture was centrifuged at 21,500 *g* for 5 minutes. The supernatant was used for radioactivity measurements in a liquid scintillation counter, whereas the residual extract was evaporated to dryness under a nitrogen stream. A 20% acetonitrile aqueous solution was then added to the residue, and the mixture was centrifuged at 21,500 *g* for 5 minutes. The resulting supernatant was analyzed by radio–high-performance liquid chromatography/MS using authentic standards for DS-1971a and M1–M13. Details of the radio–high-performance liquid chromatography/MS system are presented in Supplemental Table 1.

Calculation of DS-1971a, M1, M2, M3, M8, and M9 AUC% as a Ratio of Total Drug-Related Exposure in Humans

Based on the measured plasma radioactivity and the radiochromatograms of the plasma extracts, AUC% for DS-1971a and its major metabolites (M1, M2, M3, M8, and M9) were calculated using non-compartmental methods in WinNonlin 6.3. AUC ratios as a percentage of total radioactive exposure were calculated using the following equation:

$$AUC\ ratio\ (\%)\ in\ humans = \frac{AUC\ of\ DS-1971a, M1, M2, M3, M8,\ or\ M9\ radioactivity}{AUC\ of\ total\ radioactivity} \times 100 \quad (1)$$

Animals

Animal experiments were approved by the Institutional Animal Care and Use Committee, and performed in accordance with the animal welfare guidelines of Daiichi Sankyo Co., Ltd., which is accredited by American Association for Accreditation of Laboratory Animal Care International. Male Sprague-Dawley rats (7 weeks old) were obtained from Charles River Laboratories Japan, Inc. (Yokohama, Japan). Male cynomolgus monkeys (2-3 years old) and beagle dogs (4-5 years old) used were bred in Daiichi Sankyo Co., Ltd. (Tokyo, Japan).

Oral PK Study of DS-1971a in Rats and Dogs. DS-1971a suspended in vehicle (0.5% MC) were orally administered to rats and dogs at a dose of 10 or 1000 mg/kg (rats), or 10 mg/kg (dogs). Plasma samples were collected at 0.25, 0.5, 1, 2, 4, 7, and 24 hours post dosing, and exposure levels of DS-1971a and its metabolites (M1-M13) were determined using LC-MS/MS. PK parameters were calculated based on a non-compartmental analysis technique using WinNonlin 6.3. The AUC ratios for M1 and M2 were calculated using the following equation.

$$AUC\ ratio\ (\%)\ in\ animals = \frac{AUC\ of\ M1\ or\ M2}{Total\ AUC\ of\ DS-1971a\ and\ all\ observed\ metabolites} \times 100 \quad (2)$$

Calculation of M1 and M2 AUC% as a Ratio of Total Drug-Related Exposure in Mice and Monkeys

PK parameters of DS-1971a and the observed metabolites (i.e., M1, M2, M4, M7, M8, M11, and M13 [M13 in monkeys only]) after oral dosing of mice and monkeys with 10 and 3 mg/kg of DS-1971a, respectively, were taken from our previous study (Asano et al., 2021). The AUC ratios for M1 and M2 were calculated using the Eq. 2.

M1 and M2 Formation from DS-1971a in Chemically Deactivated HLM (SILENSOMES)

DS-1971a (1 μM) was incubated in triplicate with CYP1A2-, CYP2C8-, CYP2C9-, CYP2C19-, CYP2D6-, and CYP3A4-inactivated HLM (SILENSOMES; 0.5 mg/mL in 100 mM KPB, pH 7.4) in the presence of the NADPH-regenerating system at 37°C for 15 minutes. The final concentration of the organic solvent was $< 1\%$. After the incubation, a 50-μL aliquot of the sample was mixed with 250 μL of acetonitrile containing stable-isotope-labeled DS-1971a as an internal standard and filtered through a 0.2-μm Captiva filter (Agilent, Santa Clara, CA), and then 500 μL of water was added to the filtrate. A 7-μL aliquot of the sample was injected into the LC-MS/MS system to quantify DS-1971a, M1, and M2 concentrations. Using Microsoft Excel 2010, the quantified M1 and M2 concentrations were divided by the protein concentration of the microsomal fractions and incubation time to obtain the formation rate. The natural logarithm of DS-1971a concentration was plotted against the incubation time to determine the elimination rate constant (k_{el}) by fitting the line with the functional command "Slope" of Microsoft Excel 2010. The metabolic clearance (CL_{int}) was calculated by dividing k_{el} by the protein concentration of HLM using Microsoft Excel 2010.

M1 Formation from DS-1971a with Recombinant CYP2C8

DS-1971a (1 μM) was incubated in quadruplicate with cDNA-expressing human microsomes (0.5 mg/mL of control or CYP2C8 microsomes in 100 mM KPB, pH 7.4) in the presence of the NADPH-regenerating system at 37°C for 15 minutes. The final concentration of the organic solvent was $< 1\%$. Extraction and quantification of M1 and M2 were performed as described for HLM samples above, and their formation rates were calculated.

Metabolic Stability of M1, M2, M3, M4, and M5 in HLM or S9

M1, M2, M3, M4, or M5 (1 μM) were incubated in triplicate with HLM or human liver S9 (0.5 or 1 mg/mL in 100 mM KPB, pH 7.4) in the presence of the NADPH-regenerating system at 37°C for 10, 30, and 60 minutes. The final concentration of the organic solvent was $< 1\%$. Extraction and quantification of M1, M2, M3, M4, and M5 were performed as described for HLM samples above.

Formation of M1, M2, M3, and M5 from DS-1971a in Liver Microsomes from Mice, Rats, Dogs, Monkeys, and Humans

DS-1971a (1 μM) was incubated in triplicate with mouse, rat, dog, monkey, and human liver microsomes (0.5 mg/mL in 100 mM KPB, pH 7.4) in the presence of the NADPH-regenerating system at 37°C for 15 minutes. The final concentration of the organic solvent was $< 1\%$. Extraction and quantification of DS-1971a, M1, M2, M3, and M5 were performed as described for HLM samples above.

Toxicokinetic Evaluation of DS-1971a, M1, and M2 in 6- or 9-Month Repeated-Dose Toxicity Studies in Mice and Monkeys

Plasma samples collected 0, 0.5, 2, 6, and 24 hours or 0, 1, 2, 4, 7, and 24 hours after the last dose of 1000 mg/kg, and 10, 100, or 1000 mg/kg of DS-1971a in 6- or 9-month repeated-dose studies in male Crl:CD1(ICR) mice ($n = 3$ different mice at each sampling point) and male cynomolgus monkeys ($n = 6$ at each sampling point) were used to quantify DS-1971a, M1, and M2 exposure levels using LC-MS/MS. Toxicokinetic parameters were calculated based on a non-compartmental analysis technique using WinNonlin 6.3.

Intravenous PK Study of M1 in Rats and Monkeys

DS-1971a dissolved in vehicle (10% DMA and 90% saline) was intravenously administered to rats and monkeys (male, Sprague-Dawley and cynomolgous; $n = 3$) at a dose of 1 mg/kg. Plasma samples were collected at 0.083, 0.25, 0.5, 1, 2, 4, 7, and 24 hours later. Exposure levels of M1 were determined using LC-MS/MS and PK parameters were calculated based on a non-compartmental analysis technique using WinNonlin 6.3.

Protein Binding of M1 in Human Plasma

Protein binding rate of M1 in human plasma was determined in vitro as described previously (Shinozuka et al., 2020).

Inhibition by DS-1971a and M1 of CYP2C8 Activity

The inhibitory effect of DS-1971a and M1 on paclitaxel 6α-hydroxylating activity in HLM was determined as described previously (Yamada et al., 2020).

LC-MS/MS Analysis

LC-MS/MS analyses were performed as described previously (Asano et al., 2021).

Quantitative Structure-Activity Relationship-Based Prediction of Site of Metabolism

Quantitative structure–activity relationship (QSAR)-based metabolite predictions were made by inputting the chemical structure of DS-1971a into ADMET Predictor software 9.0 (Simulations Plus, Lancaster, CA) with site of metabolism models for P450.

Docking Simulation of the Interaction between DS-1971a and CYP2C8

Molecular docking of DS-1971a to CYP2C8 was simulated using the crystal structures of CYP2C8 (Protein Data Bank [PDB] code 2NNJ; Schoch et al., 2008) without water molecules. Three-dimensional coordinates of DS-1971a were prepared using the LigPrep module of Maestro version 12.7 (Schrödinger LLC, New York, NY). Starting with two-dimensional structures, LigPrep produces a three-dimensional structure with ionization states at pH 7. Docking simulation was performed using the standard precision mode of Glide version 9.0 (Schrödinger LLC) with the structure of CYP2C8 to obtain CYP2C8–DS-1971a docking scores and to generate a complex structure with the best docking score.

Results

PK Profiles of DS-1971a and Its Metabolites after Oral Administration of [^{14}C]DS-1971a in Humans. To identify human metabolites, plasma, urine, and feces were collected up to 192 hours after the oral administration of 400 mg [^{14}C]DS-1971a. Representative radiochromatograms of the extracts from human plasma, urine, and feces are shown in Fig. 2. The largest peak in all matrices collected was for M1, although various kinds of oxidized metabolites were also detected. The chemical structures of the detected metabolites are shown in Supplemental Fig. 1. Of these, M2 and M3 are regioisomers of M1 and M5 is a stereoisomer (Fig. 1), suggesting that the oxidation of carbon atoms at the 4 and 5 positions of the cyclohexane ring leads to four kinds of isomerized metabolites.

DS-1971a and major metabolite concentrations detected in human plasma were quantified by LC-MS/MS, and PK parameters were calculated based on non-compartmental analysis to estimate exposure levels (Fig. 3; Table 1). M1 was obviously the predominant metabolite, and its exposure level (i.e., AUC) was 1.5-fold higher than that of DS-1971a. M2 was the next most prevalent metabolite, with an exposure level (AUC) that was 58% that of the parent compound. The AUC ratios of M1 and M2 to total drug-derived materials were 27% and 10%, respectively, suggesting that these metabolites are subject to safety assessment in accordance with the MIST guidance. Because the AUC ratios of M3, M8, and M9 were each $< 5\%$, they were recognized as minor metabolites. From the structural viewpoint, M8 and M9 may be produced by AO and P450s because these metabolites were secondary metabolites of M1 and M2 (P450 metabolites) or M4 (an AO metabolite; Fig. 1).

To evaluate the DS-1971a excretion pathway in humans, radioactivity recovery after oral dosing was determined. As indicated in Table 2, 72% and 22% of radioactivity was recovered in the urine and feces, respectively, up to 168 hours after dosing, indicating that the major human elimination pathway is via urinary excretion. Based on urine concentrations, the mean (± SD) cumulative urinary excretion of DS-1971a, M1, and M2 was calculated to be 4.3 ± 2.7%, 36.0 ± 17.1%, and 10.0 ± 1.9% of the dose, respectively.

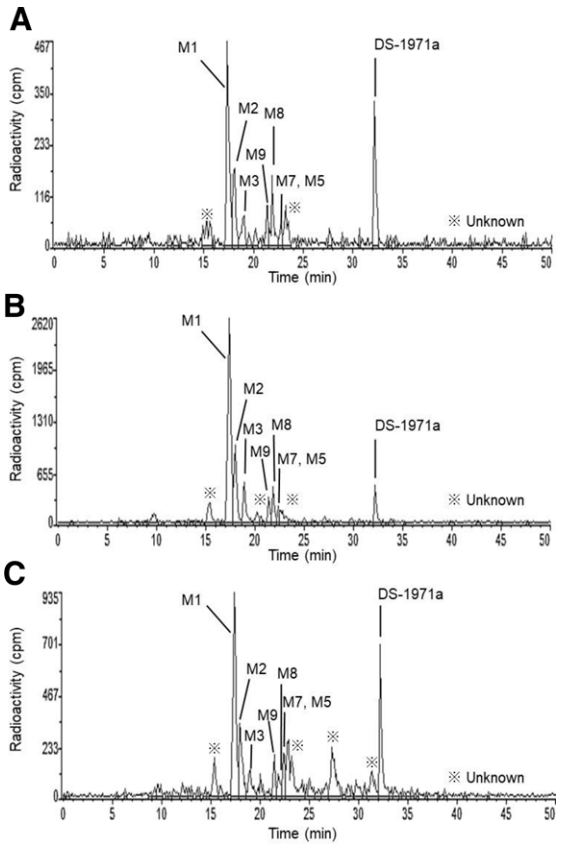

Fig. 2. Radiochromatgrams of human plasma, urine, and feces after oral administration of [^{14}C]DS-1971a. Extracts from human plasma at 6 hour (A), urine during 0–24 hours (B) and feces during 24–48 hours (C) were analyzed by radio-high-performance liquid chromatography, and the radioactive peaks of the metabolites were identified by comparing their retention times with those of authentic standards for each metabolite.

Comparison of M1 and M2 Exposure Levels between Humans and Animals. AUC% of the major metabolites M1 and M2 as a percentage of total exposure (i.e., AUC ratios) were compared between humans and experimental animals for the MIST assessment. As shown in Fig. 4, the AUC ratio of M1 was considerably higher in humans than

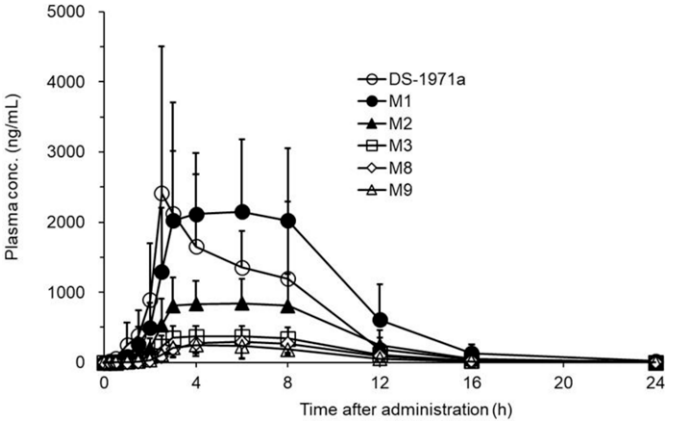

Fig. 3. Pharmacokinetic profiles of DS-1971a and its major metabolites in humans following oral administration of [^{14}C]DS-1971a. Plasma concentrations of DS-1971a, M1, M2, M3, M8, and M9 were quantified by liquid chromatography tandem mass spectrometry. Data represent the mean ± SD of six subjects.

TABLE 1

Pharmacokinetic parameters of DS-1971a, M1, M2, M3, M8, and M9 in human plasma.

Analyte	T_{max} (h)	C_{max} (ng/mL)	AUC (ng/mL·h)	$T_{1/2}$ (h)	AUC ratio (%)
DS-1971a	5.2 ± 2.2	2950 ± 1810	12500 ± 3700	13.6 ± 9.3	20.7 ± 9.5
M1	5.7 ± 2.3	3180 ± 465	18400 ± 3790	2.9 ± 0.8	26.7 ± 4.1
M2	5.7 ± 2.3	1260 ± 177	7210 ± 1600	2.3 ± 0.5	10.4 ± 1.3
M3	5.7 ± 2.3	527 ± 76.3	3160 ± 717	2.2 ± 0.4	4.6 ± 1.0
M8	6.7 ± 1.6	405 ± 157	2420 ± 839	3.1 ± 0.7	4.7 ± 1.7
M9	5.7 ± 2.3	328 ± 140	1840 ± 679	2.6 ± 0.3	4.0 ± 1.5

Data represent the mean ± SD of six subjects. Pharmacokinetic parameters (T_{max}, time to reach the maximum plasma concentration; C_{max}, maximum plasma concentration; $T_{1/2}$, terminal elimination half-life; AUC, area under the curve) were calculated using non-compartmental analysis based on the plasma concentrations of DS-1971a, M1, M2, M3, M8, and M9 determined by liquid chromatography tandem mass spectrometry. Area under the curve ratios were calculated using Eq. 1 as described in the text.

in mice, rats, dogs, and monkeys, whereas that of M2 was comparable in mice, monkeys, and humans. These findings suggest that M1 is a human disproportionate metabolite.

Furthermore, M1 exposure in humans was more than double that in mice, rats, dogs, and monkeys, but M2 exposure was lower in humans than in monkeys (Table 3). Thus, further safety assessment was considered necessary for M1, but not M2, according to the MIST guidance. It should be noted that M1 exposure in dogs was negligible.

Metabolic Stability and Chiral Inversion Study on M1, M2, M3, and M5. To investigate whether M1 and its structural isomers (M2, M3, and M5) were converted into another isomers, they were independently incubated with HLM or human liver S9 fraction in the presence of the NADPH-regenerating system. The results indicated that M1, M2, M3, and M5 were metabolically stable in HLM and human liver S9 with no declining trend (Supplemental Fig. 2, A and B). In addition, little or no chiral inversion of M1 and M5 were observed (Supplemental Fig. 2, C and D).

Species difference in M1, M2, M3, and M5 formation from DS-1971a. DS-1971a was incubated with liver microsomes from mice, rats, dogs, monkeys, and humans to evaluate the species difference in the formation of M1 and its structural isomers (M2, M3, and M5). As shown in Fig. 5, M1 was the dominant metabolite in HLM while M2 was dominant in mouse, dog, and monkey liver microsomes. In rat liver microsome, M1 and M5 were formed to a similar extent as major metabolites. The abundance of M1 was highest in HLM, followed by rat, monkey and mouse liver microsomes. M1 formation was negligible in dog liver microsome. These results confirmed species differences in the metabolism of the cyclohexane ring moiety of DS-1971a to produce M1 and its isomers.

Mechanism of M1 Formation in Humans. Previously, using in vitro systems, we demonstrated that P450s were involved in the formation of M1 and M2 in humans (Asano et al., 2021). To understand the mechanisms underlying species differences in the formation of M1, we sought to identify the P450 enzymes responsible for the formation of M1 and M2.

To evaluate the contribution of each P450 form to DS-1971a metabolism, DS-1971a was incubated with HLM that had been preincubated with a specific inhibitor for each P450 (SILENSOMES). Intrinsic clearance calculated from the DS-1971a depletion rates was markedly decreased with CYP2C8- and CYP2C9-inactivated HLM (Fig. 6A). In addition, M1 and M2 formation rates were significantly reduced with CYP2C8-inactivated HLM (Fig. 6B). Furthermore, M1 and M2 were produced with recombinant CYP2C8 (Fig. 6C). These results suggest that CYP2C8, and possibly CYP2C9, plays a crucial role in the formation of M1 and M2.

To confirm M1 formation by P450s, the ADMET Predictor, with a metabolism module that can predict metabolites using a knowledge-based QSAR model, was used to predict metabolic sites of DS-1971a. The results indicated that the site with the highest potential of being metabolized by P450s was the methyl pyrazole ring for M11 formation (Supplemental Fig. 3). However, P450-mediated M1/M2 formation was not expected to occur as the predominant metabolic pathway with this QSAR method.

We then performed docking simulation with DS-1971a and CYP2C8. The complex structure with the best docking score is shown in Fig. 7. The results suggest hydrogen bonding and/or electrostatic interactions between the pyrimidine and sulfone amide moieties of DS-1971a and Ser100, Ile102, Ile106, Thr107, and Asn217 of CYP2C8. More importantly, the results demonstrated that the cyclohexane ring was the closest to the porphyrin moiety of CYP2C8 heme. Taken together, the results of the docking simulation suggest that M1 and M2 formation is the major reaction mediated by CYP2C8.

Protein Binding of M1 in Human Plasma. Plasma protein binding of M1 in humans was 98%. High plasma protein binding of M1 was in agreement with that of DS-1971a (99%) (Shinozuka et al., 2020). These values were used to assess drug-drug interaction potential

TABLE 2

Cumulative recovery of radioactivity in the urine and feces after oral administration of [^{14}C]DS-1971 to humans at 400 mg.

	Cumulative Radioactivity Excretion (% of dose)		
Excrement	0-24 h	0-72 h	0-168 h
Urine	70.5 ± 7.5	72.1 ± 7.6	72.1 ± 7.6
Feces	0.6 ± 1.4	12.9 ± 13.5	21.9 ± 7.2
Total (urine + feces)	71.1 ± 6.6	85.0 ± 10.9	94.1 ± 1.2

Data represent the mean ± SD of six subjects.

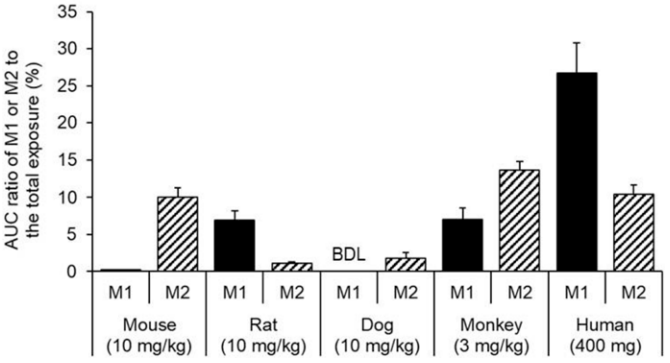

Fig. 4. Area under the curve ratios of M1 and M2 in mice, rats, dogs, monkeys, and humans. Data for M1 and M2 exposure levels in mice and monkeys after oral administration of DS-1971a were obtained from our previous report (Asano et al., 2021). Area under the curve ratios for humans and animals were calculated using Eqs. (1) and (2) as described in the text, respectively. Data represent the mean ± SD (n = 3 for mice, monkeys, rats and dogs, n = 6 for humans). BDL, below detection limit (0.1%).

TABLE 3

AUC of DS-1971a, M1, and M2 in mice, rats, dogs, monkeys, and humans.

Species (Dose)	AUC (ng·h/mL)		
	DS-1971a	M1	M2
Mouse (1000 mg/kg)[b]	30,700	235	2810
Rat (1000 mg/kg)[a]	149,000 ± 45,200	5500 ± 1160	1050 ± 581
Dog (10 mg/kg)[a]	42,900 ± 17,100	0 ± 0	859 ± 346
Monkey (1000 mg/kg)[b]	68,200 ± 40,000	5710 ± 2150	13,500 ± 4700
Human (400 mg)[a]	12,500 ± 3700	18,400 ± 3790	7210 ± 1600

Data represent the mean of three mice, and the mean ± SD in rats (n=3), dogs (n=3), monkeys (n=6), and humans (n=6).
[a]Pharmacokinetic study (single administration).
[b]Toxicokinetic study (repeated administration with safety assessment).

and contribution to efficacy by calculating the free plasma concentration of DS-1971a and M1 in humans.

Inhibitory Potential of DS-1971a and M1 on CYP2C8 Activity in HLM. Finally, inhibitory effects of DS-1971a and M1 on CYP2C8 activity in HLM were assayed with paclitaxel 6α-hydroxylation as a marker reaction. IC_{50} values of DS-1971a and M1 for the reaction were determined to be 9.2 and 60.5 μM, respectively, suggesting that DS-1971a and M1 are weak CYP2C8 inhibitors.

Discussion

Assessment of human disproportionate metabolites is important for the development of non-biologic small-molecule drugs (International Conference on Harmonization [ICH], 2010; FDA, 2020). After oral administration of radiolabeled DS-1971a, > 70% of the radioactive dose was recovered in the urine, indicating favorable oral absorption of DS-1971a in humans (Table 2). Considering that only 4% of the dose was recovered in the urine as intact DS-1971a, it was expected that most of DS-1971a administered would be eliminated via metabolism after gastrointestinal absorption.

The major metabolites in human plasma were M1 and M2, both of which appeared to require safety assessment according to the MIST guidance because their AUC ratios were > 10% of total drug-related exposure (Figs. 2, 3; Table 1). The M2 exposure level was lower in humans than in monkeys, whereas the M1 exposure level in humans exceeded that of the highest dose (1000 mg/kg) in 6- or 9-month repeated-dose toxicity studies in mice and monkeys (Table 3). Therefore, additional safety testing is not necessary for M2 but is mandatory for M1 by the initiation of "large-scale or long-duration clinical trials" (e.g., Phase 3 trials) according to the ICH M3(R2) guidance (ICH, 2010).

M1 has less pharmacological activity than DS-1971a: IC_{50} values for $Na_v1.7$ of M1 and DS-1971a were 0.31 (data not shown) and 0.02 μM

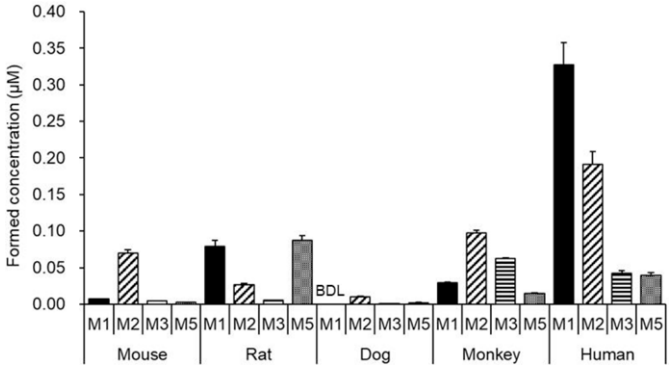

Fig. 5. The formation of M1, M2, M3, and M5 in liver microsomes from mice, rats, dogs, monkeys, and humans. DS-1971a (1 μM) was incubated for 15 minutes with mouse, rat, dog, monkey and human liver microsomes in the presence of the nicotinamide adenine dinucleotide phosphate -regenerating system. After incubation, M1, M2, M3, and M5 concentrations were quantified by liquid chromatography tandem mass spectrometry. Data represent the mean ± SD of three incubations. BDL, below detection limit (0.0003 μM).

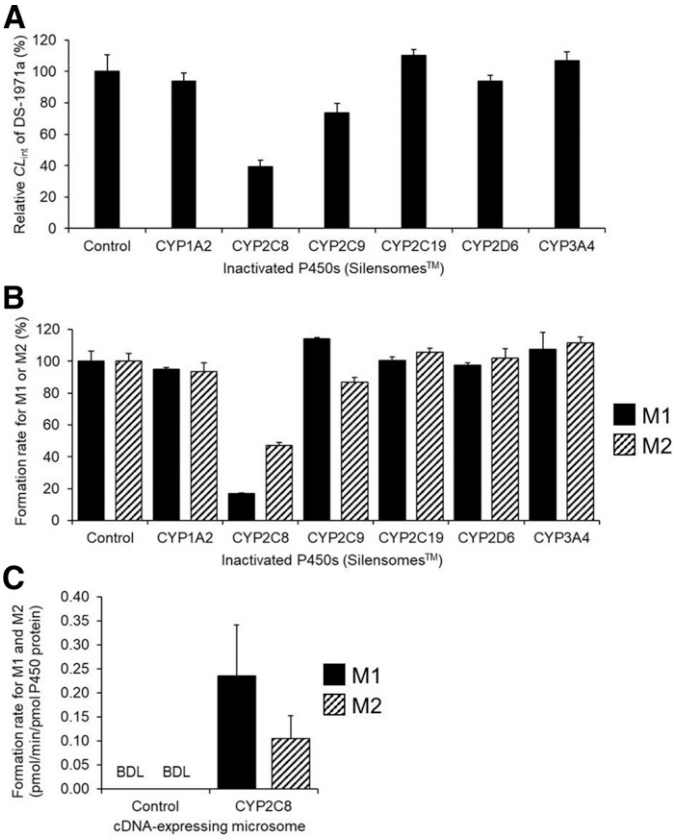

Fig. 6. Identification of P450 enzymes responsible for M1 and M2 formation. (A,B) DS-1971a (1 μM) was incubated for 15 minutes with control human liver microsome (HLM) or HLM pretreated with a specific P450 inhibitor in the presence of an nicotinamide adenine dinucleotide phosphate -regenerating system. (A) Relative intrinsic clearance of DS-1971a was calculated, with that of the control HLM set to 100%. Data represent the mean ± SD of three incubations. (B) M1 and M2 concentrations after 15-minute incubation were determined by liquid chromatography tandem mass spectrometry. Data represent the mean ± SD of relative formation rates of M1 and M2, with that of the control HLM set to 100% (n = 3 incubations). (C) DS-1971a (1 μM) was incubated with recombinant CYP2C8 for 15 minutes in the presence of the nicotinamide adenine dinucleotide phosphate -generating system. The formation rates of M1 and M2 were calculated based on the M1 and M2 concentrations determined by liquid chromatography tandem mass spectrometry. Data represent the mean ± SD of four incubations. BDL, below detection limit (0.01 pmol/min/pmol P450 protein).

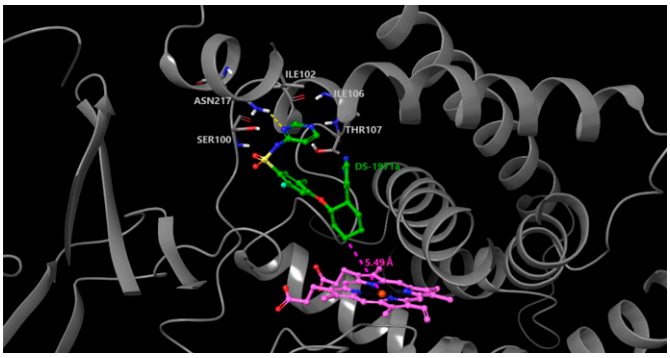

Fig. 7. Docking model of DS-1971a and CYP2C8. DS-1971a is shown in green, heme is shown in pink, and the amino acid residues of CYP2C8 that have characteristic interactions with DS-1971a are shown as a tube model. The overall structure of CYP2C8 is shown as a ribbon model. The distance from the carbon atom at the 5 position of the cyclohexane ring of DS-1971a to the heme iron of CYP2C8 is 5.49 Å.

(Shinozuka et al., 2020), indicating the minimal contribution of M1 to human efficacy because its maximum free plasma concentration at 400 mg (0.13 μM) was below the IC_{50} value. M1 exposure in monkeys (5710 ng·h/mL) at a dose of 1000 mg/kg was relatively close to that in humans (18400 ng·h/mL), but we have not explored doses over 1000 mg/kg because a limit dose is set as 1000 mg/kg when saturated exposure (Supplemental Table 2) is observed in the ICH M3(R2) guidance (ICH, 2010).

This work shed light on the possible mechanism for disproportionate metabolite based on in vitro and vivo formation of M1. Four types of metabolites monoxidized at the cyclohexane ring of DS-1971a (M1, M2, M3, and M5) were detected in human plasma, urine, and feces (Supplemental Fig. 1), with these metabolites having regio- or stereoisomeric relationships (Fig. 1). Since little or no chiral inversion of these isomers was confirmed (Supplemental Fig. 2), these metabolites were formed by P450s in a regio- or stereospecific manner. Some drugs, such as glipizide and glibenclamide, also possess a cyclohexane ring, and the formation of their isomerized hydroxylated P450 metabolites was reported (Rupp et al., 1969; Sugihara and Sato, 1975; Zharikova et al., 2007 and 2009; El-Haj and Ahmed, 2020). Incubation of DS-1971a with liver microsomes from various species suggested that HLM showed the highest metabolic activity to form M1, and the dominant metabolite in mouse, rat, monkey, and dog liver microsome included metabolites other than M1 (i.e., M2, M1/M5, M2, and M2, respectively) (Fig. 5). Although rat and monkey P450 exhibited the second and third highest M1 formation activity, M1 exposures in rats and monkeys, even at 1000 mg/kg, were smaller than that in humans (Table 3), likely due to relatively low exposure (AUC) of DS-1971a and M1 for their doses in toxicity study (Supplemental Table 2), and species differences in the PK profiles of M1. In fact, the clearance rate (*CL*) of M1 was much slower in monkeys than rats (Supplemental Table 3), while M1 formation activity was higher in rats than monkeys (Fig. 5), which leads to comparable M1 exposure between them (Table 3). Metabolite exposure basically depends on not only the produced amount but their *CL* (Obach et al., 2018). If M1 *CL* was smaller in rats or absorption was not saturated at 1000 mg/kg in monkeys, M1 exposure in humans might be covered by either of the animals. Thus, the case study with M1 illustrates the importance of the quantitative understanding and prediction of metabolite exposure in animals and humans.

CYP2C8 was identified as a metabolizing enzyme responsible for M1 formation in humans by incubation studies with SILENSOMES (Parmentier et al., 2017, 2019) and recombinant enzymes (Fig. 6). CYP2C8 is one of the major human P450s metabolizing xenobiotic and endogenous compounds, such as paclitaxel, amodiaquine, arachidonic acid, and retinoids. Concomitant administration of a CYP2C8 inhibitor, such as gemfibrozil, significantly increased the exposure levels of CYP2C8 substrates, including repaglinide and pioglitazone (Lai et al., 2009). These facts suggest potential drug-drug interaction (DDI) risk of DS-1971a as a victim drug. On the other hand, DDI potential of DS-1971a as a perpetrator drug was suggested to be low because the maximum free plasma concentration of DS-1971a and M1 at a dose of 400 mg were 0.06 and 0.13 μM, respectively, and they were more than 100-fold less than their IC_{50} values (9.2 μM for DS-1971a and 60.5 μM for M1).

Our results also give rise to novel insight into species difference in CYP2C8 metabolism. In vitro incubation studies and PK evaluation demonstrated M1 formation in mice, rats, and monkeys but not in dogs (Figs. 4 and 5), indicating that the metabolic activity was impaired in dogs. It is known that dog CYP2C enzymes, CYP2C21 and CYP2C41, show low homologies (67–83%) to human CYP2Cs (Martignoni et al., 2006) and CYP2C9 and CYP2C19 substrates were differently metabolized in dogs and humans (Graham et al., 2003). Meanwhile, monkey CYP2Cs show the highest homology (> 90%) to human CYP2Cs among animals. However, M1 formation activity in monkeys was much less than that in humans (Fig. 5), which is consistent with a much slower metabolic rate of paclitaxel 6α-hydroxylation by CYP2C8 in monkeys than humans (Yoda et al., 2012; Emoto et al., 2013). Thus, our observation would raise the caution about CYP2C8-specific substrates because exposure levels of their metabolites in humans might exceed those in animals.

Recently, we reported that the major metabolic pathway of DS-1971a in humans was assumed to be the P450-mediated M1 formation (Asano et al., 2021). In the present study, we demonstrated that M1 was the most abundant metabolite in human plasma, and AO-related metabolites M8 and M9 were minor metabolites in humans (Table 1 and Fig. 2). When M1, M2, and M4, possible first-step metabolites of M8 and M9, were incubated with HLM or human liver S9 fraction in the presence of NADPH, no further metabolism of M1 and M2 was observed, but M4 was rapidly metabolized (Supplemental Fig. 2) into dioxides including M8 and M9 (data not shown). Therefore, the primary metabolism leading to the formation of M8 and M9 may be M4 formation by AO. These results suggest that AO and P450s make minor and major contributions, respectively, to the metabolic clearance of DS-1971a in humans.

There are two in silico approaches to predict the site of metabolism: QSAR and docking simulation. Although the QSAR method is useful for predicting metabolites (Clark, 2018), it alone was not sufficient for predicting the formation of M1 and M2 as major metabolites (Supplemental Fig. 3), and so we performed structural modeling. Using structural information on the complex of felodipine and CYP2C8 at a resolution of 2.3 Å (PDB ID: 2NNJ), docking simulation between CYP2C8 and DS-1971a yielded a complex structure with the best docking score in which the cyclohexane ring moiety of DS-1971a was located very close to the heme iron of CYP2C8 (Fig. 7). When a general cut-off distance from a carbon atom to be metabolized to the heme iron of < 6 Å (Yuki et al., 2012; Sato et al., 2017) was applied, carbons at both the 4 and 5 positions of the cyclohexane ring were highly likely sites of CYP2C8-dependent metabolism, which is consistent with the formation of M1 and M2.

Critical interactions were suggested by this docking structure between the pyrimidine ring and sulfonamide bond of DS-1971a and Ser100, Ile102, Ile106, Thr107, and Asn217 of CYP2C8. It is reasonable that all these amino acid residues are located at the active site of CYP2C8 (i.e., Ser100, Ile102, Ile106, and Thr107 are from helix B′, Asn217 is from helix F′; Schoch et al., 2004). The only difference in these amino acid

residues between human and monkey CYP2C8 is a Ser100 substitution with Leu in monkeys (Komori et al., 1992). Because the replacement of Ser100 with Ala resulted in a drastic decrease in paclitaxel metabolism (Melet et al., 2004), the absence or presence of the interaction of DS-1971a with Ser100 might be a cause of species different formation of M1 between humans and monkeys. Further, we compared the CYP2C8-bound structure of DS-1971a with that of montelukast (PDB ID: 2NNI; Supplemental Fig. 4); the overlaid structures indicate that Ser100 and Asn217 are the important amino acid residues that interact with CYP2C8 for both compounds.

In conclusion, we have demonstrated that M1 is the predominant and human disproportionate metabolite of DS-1971a, and that it requires further safety assessment. CYP2C8 plays a critical role in the formation of M1. Hydrogen bonding and/or electrostatic interactions of the pyrimidine and sulfonamide moieties of DS-1971a with several amino acids in the CYP2C8 active site would move the cyclohexane ring closer to the heme iron. This is the first report of a human disproportionate metabolite generated by CYP2C8-mediated primary metabolism.

Acknowledgments

The authors thank Schrödinger, Inc. and Simulation Plus for their generous support with the in silico analysis. The authors also appreciate Ryo Yamanaka for performing the pharmacokinetic study in dogs.

Author Contributions

Participated in research design: Asano, Zahir, Shiozawa, Nishiya, Kimura, Yamamura, Yoshinari.

Conducted experiments: Asano, Shiozawa, Nishiya, Kazui, Shinozuka, T. Watanabe.

Performed data analysis: Asano, Hamaue, Zahir, Ikeguchi, Yahara.

Wrote or contributed to the writing of the manuscript: Asano, Hamaue, Shiozawa, Kimura, Shibayama, Inoue, N. Watanabe, Yoshinari.

References

Anderson S, Luffer-Atlas D, and Knadler MP (2009) Predicting circulating human metabolites: how good are we? *Chem Res Toxicol* **22**:243–256.

Asano D, Shibayama T, Shiozawa H, Inoue SI, Shinozuka T, Murata S, Watanabe N, and Yoshinari K (2021) Evaluation of species differences in the metabolism of the selective $Na_V1.7$ inhibitor DS-1971a, a mixed substrate of cytochrome P450 and aldehyde oxidase. *Xenobiotica* **51**:1060–1070.

Callegari E, Varma MVS, and Obach RS (2020) Prediction of metabolite-to-parent drug exposure: derivation and application of a mechanistic static model. *Clin Transl Sci* **13**:520–528.

Clark RD (2018) Predicting mammalian metabolism and toxicity of pesticides in silico. *Pest Manag Sci* **74**:1992–2003.

Dalvie D, Obach RS, Kang P, Prakash C, Loi CM, Hurst S, Nedderman A, Goulet L, Smith E, Bu HZ, et al. (2009) Assessment of three human in vitro systems in the generation of major human excretory and circulating metabolites. *Chem Res Toxicol* **22**:357–368.

Duley JA, Harris O, and Holmes RS (1985) Analysis of human alcohol- and aldehyde-metabolizing isozymes by electrophoresis and isoelectric focusing. *Alcohol Clin Exp Res* **9**:263–271.

El-Haj BM and Ahmed SBM (2020) Metabolic-hydroxy and carboxy functionalization of alkyl moieties in drug molecules: prediction of structure influence and pharmacologic activity. *Molecules* **25**:1937.

Emoto C, Yoda N, Uno Y, Iwasaki K, Umehara K, Kashiyama E, and Yamazaki H (2013) Comparison of p450 enzymes between cynomolgus monkeys and humans: p450 identities, protein contents, kinetic parameters, and potential for inhibitory profiles. *Curr Drug Metab* **14**:239–252.

Food and Drug Administration (FDA) (2020) *Guidance for industry: Safety Testing of Drug Metabolites*, Center for Drug Evaluation and Research, U.S. Food and Drug Administration, U.S. Department of Health and Human Services, Silver Spring, MD.

Graham MJ, Bell AR, Crewe HK, Moorcraft CL, Walker L, Whittaker EF, and Lennard MS (2003) mRNA and protein expression of dog liver cytochromes P450 in relation to the metabolism of human CYP2C substrates. *Xenobiotica* **33**:225–237.

Gross G and Wilson I (2009) Issues in the safety testing of metabolites. *Future Med Chem* **1**:1381–1390.

International Conference on Harmonisation (ICH) (2010) M3(R2) Guidance: Nonclinical Safety Studies for the Conduct of Human Clinical Trials and Marketing Authorization for Pharmaceuticals. ICH, Geneva, Switzerland.

Komori M, Kikuchi O, Sakuma T, Funaki J, Kitada M, and Kamataki T (1992) Molecular cloning of monkey liver cytochrome P-450 cDNAs: similarity of the primary sequences to human cytochromes P-450. *Biochim Biophys Acta* **1171**:141–146.

Lai XS, Yang LP, Li XT, Liu JP, Zhou ZW, and Zhou SF (2009) Human CYP2C8: structure, substrate specificity, inhibitor selectivity, inducers and polymorphisms. *Curr Drug Metab* **10**:1009–1047.

Lutz JD, Fujioka Y, and Isoherranen N (2010) Rationalization and prediction of in vivo metabolite exposures: the role of metabolite kinetics, clearance predictions and in vitro parameters. *Expert Opin Drug Metab Toxicol* **6**:1095–1109.

Martignoni M, Groothuis GM, and de Kanter R (2006) Species differences between mouse, rat, dog, monkey and human CYP-mediated drug metabolism, inhibition and induction. *Expert Opin Drug Metab Toxicol* **2**:875–894.

Melet A, Marques-Soares C, Schoch GA, Macherey AC, Jaouen M, Dansette PM, Sari MA, Johnson EF, and Mansuy D (2004) Analysis of human cytochrome P450 2C8 substrate specificity using a substrate pharmacophore and site-directed mutants. *Biochemistry* **43**:15379–15392.

Nguyen HQ, Kimoto E, Callegari E, and Obach RS (2016) Mechanistic modeling to predict midazolam metabolite exposure from in vitro data. *Drug Metab Dispos* **44**:781–791.

Obach RS, Lin J, Kimoto E, Duvvuri S, Nicholas T, Kadar EP, Tremaine LM, and Sawant-Basak A (2018) Estimation of circulating drug metabolite exposure in human using in vitro data and physiologically based pharmacokinetic modeling: Example of a high metabolite/parent drug ratio. *Drug Metab Dispos* **46**:89–99.

Parmentier Y, Pothier C, Delmas A, Caradec F, Trancart MM, Guillet F, Bouaita B, Chesne C, Brian Houston J, and Walther B (2017) Direct and quantitative evaluation of the human CYP3A4 contribution (f_m) to drug clearance using the in vitro SILENSOMES model. *Xenobiotica* **47**:562–575.

Parmentier Y, Pothier C, Hewitt N, Vincent L, Caradec F, Liu J, Lin F, Trancart MM, Guillet F, Bouaita B, et al. (2019) Direct and quantitative evaluation of the major human CYP contribution (fmCYP) to drug clearance using the in vitro Silensomes™ model. *Xenobiotica* **49**:22–35.

Rupp W, Christ O, and Heptner W (1969). Resorption, excretion and metabolism after intravenous and oral administration of HB 419-14C in man. *Arzneimittelforschung* **19**:1428–1434 in German.

Sato A, Yuki H, Watanabe C, Saito J, Konagaya A, and Honma T (2017) Prediction of the site of CYP3A4 metabolism of tolterodine by molecular dynamics simulation from multiple initial structures of the CYP3A4–tolterodine complex. *Chem-Bio Informatics J* **17**:38–52.

Schadt S, Bister B, Chowdhury SK, Funk C, Hop CECA, Humphreys WG, Igarashi F, James AD, Kagan M, Khojasteh SC, et al. (2018) A decade in the MIST: Learnings from investigations of drug metabolites in drug development under the "Metabolites in Safety Testing" regulatory guidance. *Drug Metab Dispos* **46**:865–878.

Schoch GA, Yano JK, Sansen S, Dansette PM, Stout CD, and Johnson EF (2008) Determinants of cytochrome P450 2C8 substrate binding: structures of complexes with montelukast, troglitazone, felodipine, and 9-*cis*-retinoic acid. *J Biol Chem* **283**:17227–17237.

Schoch GA, Yano JK, Wester MR, Griffin KJ, Stout CD, and Johnson EF (2004) Structure of human microsomal cytochrome P450 2C8. Evidence for a peripheral fatty acid binding site. *J Biol Chem* **279**:9497–9503.

Sharma R, Litchfield J, Atkinson K, Eng H, Amin NB, Denney WS, Pettersen JC, Goosen TC, Di L, Lee E, et al. (2014) Metabolites in safety testing assessment in early clinical development: a case study with a glucokinase activator. *Drug Metab Dispos* **42**:1926–1939.

Shinozuka T, Kobayashi H, Suzuki S, Tanaka K, Karanjule N, Hayashi N, Tsuda T, Tokumaru E, Inoue M, Ueda K, et al. (2020) Discovery of DS-1971a, a potent, selective $Na_V1.7$ inhibitor. *J Med Chem* **63**:10204–10220.

Sugihara J and Sato H (1975) The biological fate of glipizide (II). The metabolism of glipizide in animals. *Radioisotopes* **24**:167–173.

Surapaneni S, Yerramilli U, Bai A, Dalvie D, Brooks J, Wang X, Selkirk JV, Yan YG, Zhang P, Hargreaves R, et al. (2021) Absorption, metabolism, and excretion, in vitro pharmacology, and clinical pharmacokinetics of ozanimod, a novel sphingosine 1-phosphate receptor modulator. *Drug Metab Dispos* **49**:405–419.

Yamada M, Ishizuka T, Inoue SI, Rozehnal V, Fischer T, and Sugiyama D (2020) Drug-Drug Interaction Risk Assessment of Esaxerenone as a Perpetrator by In Vitro Studies and Static and Physiologically Based Pharmacokinetic Models. *Drug Metab Dispos* **48**:769–777.

Yoda N, Emoto C, Date S, Kondo S, Miyake M, Nakazato S, Umehara K, and Kashiyama E (2012) Characterization of intestinal and hepatic P450 enzymes in cynomolgus monkeys with typical substrates and inhibitors for human P450 enzymes. *Xenobiotica* **42**:719–730.

Yuki H, Honma T, Hata M, and Hoshino T (2012) Prediction of sites of metabolism in a substrate molecule, instanced by carbamazepine oxidation by CYP3A4. *Bioorg Med Chem* **20**:775–783.

Zharikova OL, Fokina VM, Nanovskaya TN, Hill RA, Mattison DR, Hankins GD, and Ahmed MS (2009) Identification of the major human hepatic and placental enzymes responsible for the biotransformation of glyburide. *Biochem Pharmacol* **78**:1483–1490.

Zharikova OL, Ravindran S, Nanovskaya TN, Hill RA, Hankins GD, and Ahmed MS (2007) Kinetics of glyburide metabolism by hepatic and placental microsomes of human and baboon. *Biochem Pharmacol* **73**:2012–2019.

Zheng J, Xin Y, Zhang J, Subramanian R, Murray BP, Whitney JA, Warr MR, Ling J, Moorehead L, Kwan E, et al. (2018) Pharmacokinetics and disposition of momelotinib revealed a disproportionate human metabolite-resolution for clinical development. *Drug Metab Dispos* **46**:237–247.

Zientek M, Jiang Y, Youdim K, and Obach RS (2010) In vitro-in vivo correlation for intrinsic clearance for drugs metabolized by human aldehyde oxidase. *Drug Metab Dispos* **38**:1322–1327.

Address correspondence to: Daigo Asano, Daiichi Sankyo Co., Ltd., 1-2-58, Hiromachi, Shinagawa-ku, Tokyo, 140-8710, Japan. E-mail: asano.daigo.vi@daiichisankyo.co.jp

Drug Metabolism and Disposition
Manuscript number: DMD-AR-2021-000665

Title page

CYP2C8-Mediated Formation of a Human Disproportionate Metabolite of the Selective $Na_V1.7$ Inhibitor DS-1971a, a Mixed Cytochrome P450 and Aldehyde Oxidase Substrate

Daigo Asano, Syoya Hamaue, Hamim Zahir, Hideyuki Shiozawa, Yumi Nishiya, Takako Kimura, Miho Kazui, Naotoshi Yamamura, Marie Ikeguchi, Takahiro Shibayama, Shin-ichi Inoue, Tsuyoshi Shinozuka, Toshiyuki Watanabe, Chizuko Yahara, Nobuaki Watanabe, and Kouichi Yoshinari

Affiliations

Drug Metabolism and Pharmacokinetics Research Laboratories, Daiichi Sankyo Co., Ltd., Tokyo, Japan (D.A., H.S., Y.N., M.K., N.Y., T. Shibayama, S.I., C.Y., N.W.); Organic & Biomolecular Chemistry Department, Daiichi Sankyo RD Novare Co., Ltd., Tokyo, Japan (S.H., T.K.); Quantitative Clinical Pharmacology and Translational Sciences, Daiichi Sankyo, Inc., Basking Ridge, New Jersey (H.Z.); Translational Science Department, Daiichi Sankyo Co., Ltd., Tokyo, Japan (M.I.); R&D Planning & Management Department, Daiichi Sankyo Co., Ltd., Tokyo, Japan (T. Shinozuka); Medicinal Safety Research Laboratories, Daiichi Sankyo Co., Ltd., Tokyo, Japan (T.W.); Laboratory of Molecular Toxicology, School of Pharmaceutical Sciences, University of Shizuoka, Shizuoka, Japan (K.Y.)

Supplementary Data

Supplementary Table S1. Details of the Radio-HPLC/MS System Used in This Study

Radio detector	
Apparatus	Radiomatic 625TR (PerkinElmer, Inc.)
Detection	Radioactivity (^{14}C), UV (280 nm)
Liquid scintillator	Ultima-Flo M (PerkinElmer, Inc.)
Flow-rate of liquid scintillator	3 mL/min, mixed with the eluate from HPLC
HPLC/MS system	
Apparatus	Accela/LTQ Orbitrap XL (Thermo Fisher Scientific Inc.)
Flow-rate of mobile phase	1 mL/min
Mobile phase	A, water containing 0.1% (v/v) formic acid; B, acetonitrile containing 0.1% (v/v) formic acid
Gradient elution program	B: 15% (0 min) – 20% (15 min) – 50% (35 min) – 95% (40 min) – 95% (45 min) – 15% (45.1 min) – 15% (50 min)
Column	Inertsil ODS-3 (4.6 mm × 150 mm, S-3 μm, GL Sciences Inc.)
Column temperature	40°C
Ionization mode	ESI (electrospray ionization), positive
MS mode	CID (collision-induced dissociation; fragment ions generated in ion trap) and HCD (higher energy collisional dissociation; fragment ions generated in collision cell)
Collision energy	CID: 35%; HCD: 35%
Capillary temperature	350°C
Spray voltage	5.00 kV
Capillary voltage	12 V
Tube Lens	100 V

Supplementary Table S2. Exposure to DS-1971a and M1 at Various Doses in 9-Month Repeated-Dose Toxicity Studies of DS-1971a in Monkeys

Species (Dose)	AUC (ng·h/mL)	
	DS-1971a	M1
10 mg/kg	8980 ± 920	1080 ± 310
100 mg/kg	19900 ± 4300	2850 ± 650
1000 mg/kg	44700 ± 19800	5710 ± 2150

Data represent the mean ± SD in monkeys (n=4 for 10 and 100 mg/kg, and n=6 for 1000 mg/kg)

Supplementary Table S3. PK Parameters of M1 in Rats and Monkeys after Intravenous Administration of M1 at a Dose of 1 mg/kg

Species	*CL* (mL/min/kg)	Vd_{ss} (L/kg)
Rats	153 ± 23	2.3 ± 1.4
Monkeys	8.1 ± 3.7	0.2 ± 0.1

PK parameters were calculated based on the concentrations determined in plasma, which were collected 0.083, 0.25, 0.5, 1, 2, 4, 7 and 24 h after the intravenous administration of M1 (1 mg/kg) using non-compartmental analysis. Each value represents the mean ± SD of three rats or monkeys.

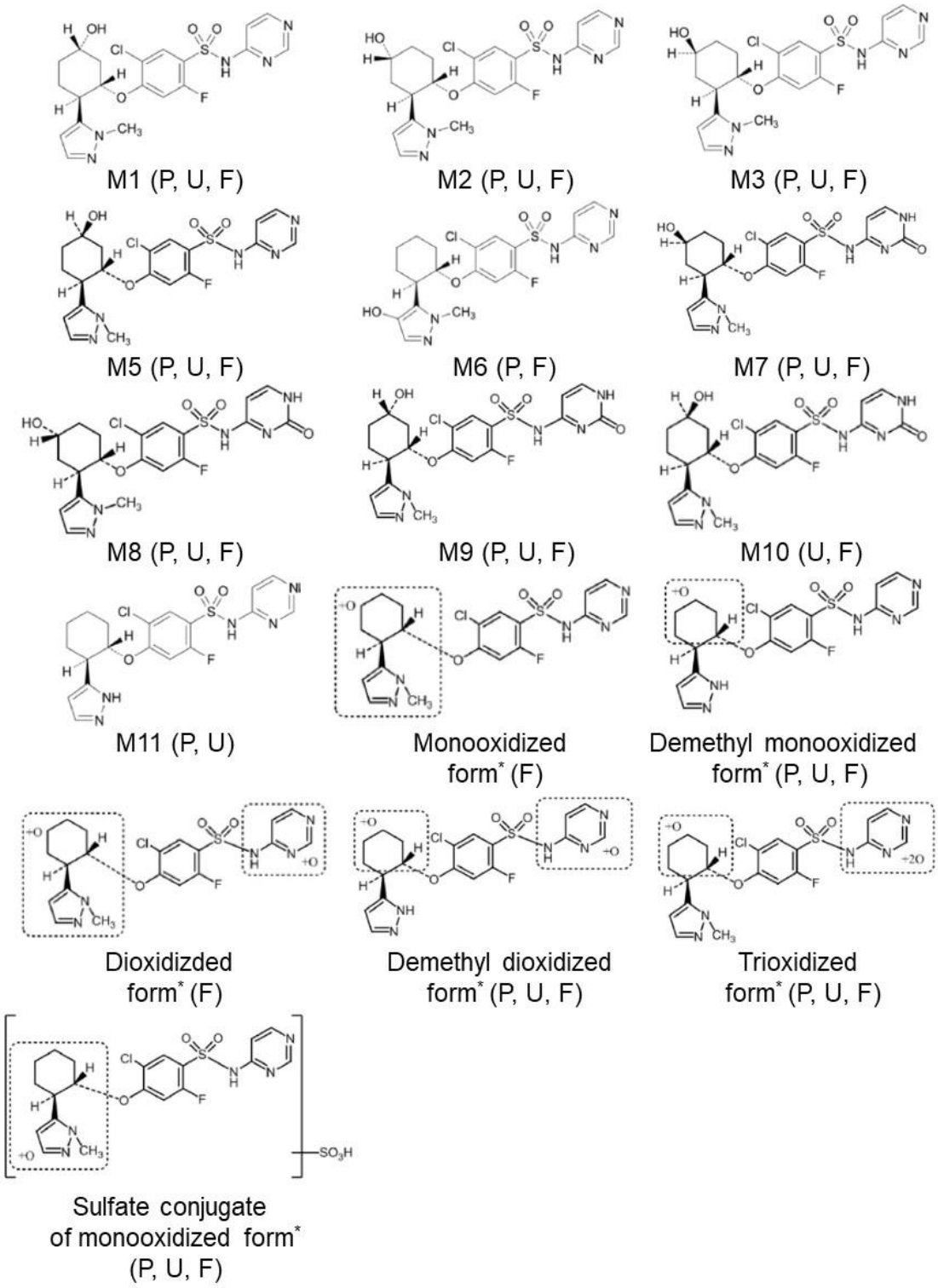

Supplementary Fig. S1. Metabolites detected in human plasma, urine, and feces.

P, plasma; U, urine; F, feces. *, definitive structures are unknown due to the lack of the authentic standards.

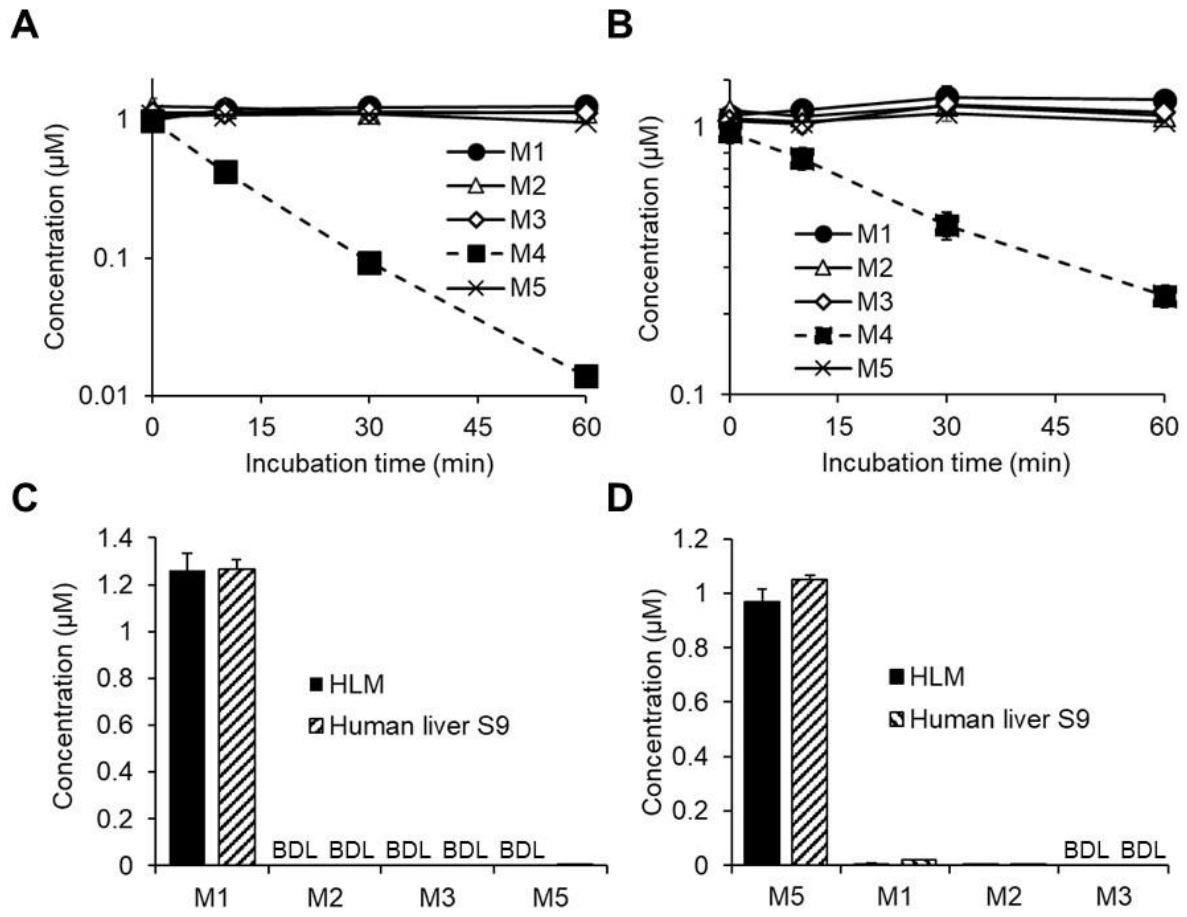

Supplementary Fig. S2. Metabolic stability of M1, M2, M3, M4, and M5 in HLM (A) and human liver S9 fraction (B), and chiral inversion of M1 (C) and M5 (D).

M1, M2, M3, M4, and M5 (1 μM) were incubated with HLMs (0.5 mg/mL) or human liver S9 fraction (1 mg/mL) in the presence of the NADPH-regenerating system, and their concentrations were determined by LC-MS/MS. Remaining concentrations of M1, M2, M3, M4, and M5 in HLM (A) or human liver S9 (B) during 60-min incubation are plotted in a semi-logarithmic scale. The concentrations of M1, M2, M3, and M5 after 60-min incubation of M1 (C) or M5 (D) are presented as bar graphs. Data represent the mean ± SD of three incubations. BDL, below detection limit (0.0025 μM).

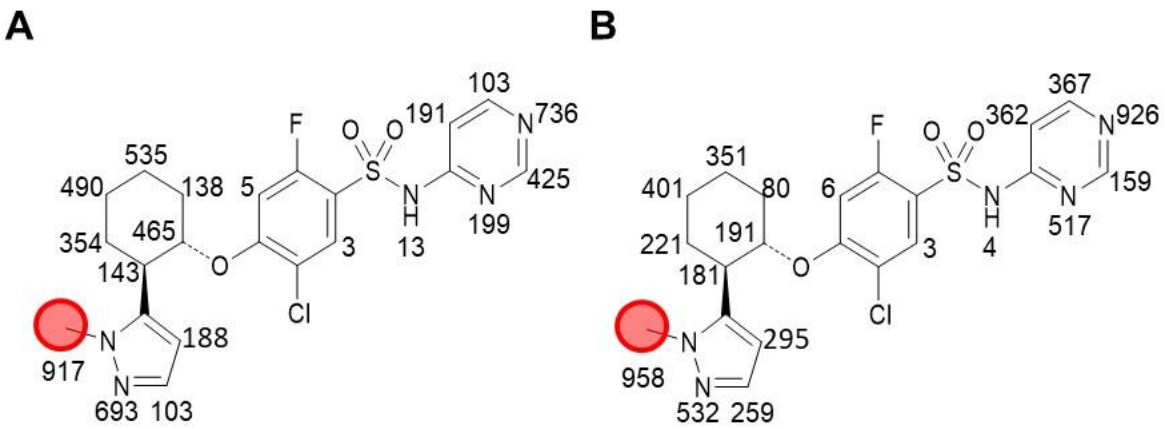

Supplementary Fig. S3. QSAR-predicted sites of metabolism mediated by CYP2C8 and CYP2C9.

QSAR analysis was performed with ADMET Predictor™ software with a metabolism module to calculate the probability of (A) CYP2C8- and (B) CYP2C9-mediated metabolism. The numbers adjacent to atoms represent the likelihood of metabolism that ranges from 1 to 1000, with 1000 being the greatest likelihood. Atoms with a score of zero (0) are not labeled. The atoms highlighted with a red circle are the predicted sites of metabolism with maximum probability for each enzyme system.

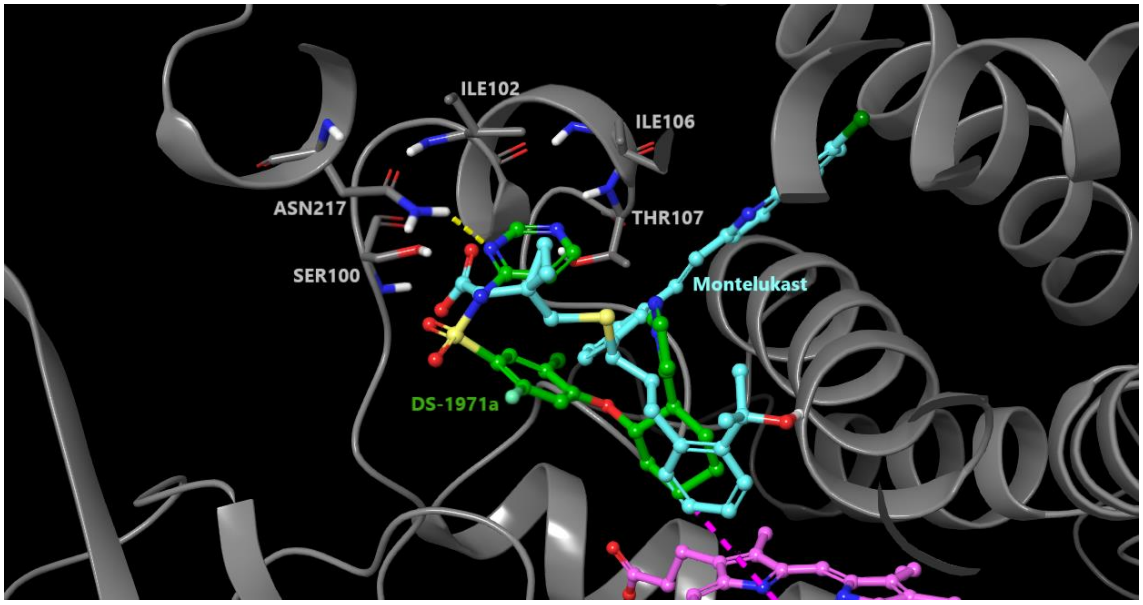

Supplementary Fig. S4. Superimposition of CYP2C8-bound DS-1971a (green) and montelukast (cyan) with CYP2C8.

The structure information for the montelukast–CYP2C8 complex was obtained from PDB 2NNI.